

# Assessment of the Gaussian Covariance Approximation over an Earth-Asteroid Encounter Period

By Daniel Mattern <sup>1)</sup>

<sup>1)</sup>Omitron, Inc., Beltsville, MD | NASA Goddard Space Flight Center, Flight Dynamics Facility, Greenbelt, MD

In assessing the risk an asteroid may pose to the Earth, the asteroid's state is often predicted for many years, often decades. Only by accounting for the asteroid's initial state uncertainty can a measure of the risk be calculated. With the asteroid's state uncertainty growing as a function of the initial velocity uncertainty, orbit velocity at the last state update, and the time from the last update to the epoch of interest, the asteroid's position uncertainties can grow to many times the size of the Earth when propagated to the encounter "risk corridor." This paper examines the merits of propagating the asteroid's state covariance as an analytical matrix. The results of this study help to bound the efficacy of applying different metrics for assessing the risk an asteroid poses to the Earth. Additionally, this work identifies a criterion for when different covariance propagation methods are needed to continue predictions after an Earth-encounter period.

**Key Words:** planetary defense, uncertainty characterization, asteroid

## Nomenclature

|               |                                  |
|---------------|----------------------------------|
| $PHA$         | : potentially hazardous asteroid |
| $TCA$         | : time of closest approach       |
| $NEA$         | : near-Earth asteroid            |
| $P_c$         | : probability of collision       |
| $D_{MH}$      | : Mahalanobis distance           |
| $SOI$         | : sphere of influence            |
| $R_{sc}$      | : characteristic scale ratio     |
| $\alpha$      | : albedo                         |
| $H$           | : absolute magnitude             |
| $D$           | : asteroid diameter              |
| $\varepsilon$ | : orbit energy                   |
| $v$           | : orbit velocity                 |
| $r$           | : orbit radius                   |
| $G$           | : gravitational constant         |
| $M$           | : mass of the central body       |
| $\Delta$      | : finite difference              |
| $\sigma$      | : standard deviation             |
| $C_{QF}$      | : covariance quality factor      |

## 1. Introduction

Many metrics exist for assessing the risk a potential hazardous asteroid (PHA) may pose to the Earth.<sup>†</sup> A fundamental issue with any metric is generally the scale of the asteroid's position uncertainty when propagated to the time of closest approach (TCA) with the Earth. As PHAs generally have orbits somewhat similar to Earth, their synodic period is often multi-year or even decades-long. As such, any initial measurement uncertainty is very large when propagated to TCA.

Two common metrics that are used to assess a

collision risk are the probability of collision ( $P_c$ ) and Mahalanobis distance ( $D_{MH}$ ).<sup>1,2)</sup> Large uncertainties generally affect  $P_c$  calculations by returning negligible values early on and by returning false positives with subsequent measurements (described later). Mahalanobis distance calculations are affected by large uncertainties predominantly based on how close the distribution gets to the Earth's gravitational sphere of influence (SOI). Because  $D_{MH}$  calculations require the uncertainty distribution to be approximated by a covariance matrix, this matrix imposes Gaussian assumptions on the distribution in the coordinate frame in

<sup>†</sup>PHAs are defined as near-Earth objects whose minimum orbit intersection distance with the Earth is 0.05 AU or less and whose absolute magnitude is 22.0 or brighter.

which the matrix is represented.[2] These assumptions are challenged when the distribution is propagated through a significant gravitational gradient.

This paper examines the appropriate domains for using  $D_{MH}$  or  $P_c$  to assess an asteroid's impact risk. Often, the difficulty of calculating  $P_c$  is the necessity to use a large-scale Monte Carlo approximation of the covariance matrix, which is computationally expensive and often time-consuming. Conversely,  $D_{MH}$  can be calculated by propagating the 6x6 position matrix using a standard state-transition matrix. As such, this paper identifies a criterion – called the characteristic scale ratio ( $R_{sc}$ ) – for determining which metric is more appropriate.

## 2. Background

### 2.1. Observability and Orbit Determination

While many small asteroids strike the Earth frequently without serious consequence, the threat posed by asteroids only tens of meters in size is non-trivial. In 2013, a 20-meter asteroid exploded roughly 30 km over Chelyabinsk, Russia. The resulting shock wave damaged nearly 7,200 buildings and injured over 1,500 people. Current NEO population estimates predict there are nearly 10 million NEOs larger than the Chelyabinsk asteroid that are yet undiscovered.<sup>3)</sup> The Tunguska event in 1908 flattened nearly 500,000 acres of forest in the uninhabited area of the Eastern Siberian Taiga. That asteroid was estimated to be roughly 40 meters in diameter. A similarly sized, denser asteroid created a nearly 1 mile wide crater in the Arizona desert 50,000 years ago. Current estimates of undiscovered NEOs larger than 40 meters exceeds 300,000.<sup>3)</sup>

In 2005, the United States Congress directed a survey to find 90% of all NEOs with diameters larger than 140 meters by 2020. Such asteroids, were they to impact Earth, would release more energy than the largest nuclear weapon ever tested. As of 2017, only 28% of asteroids larger than 140 meters have been discovered - the primary detection difficulty stemming from the limited observability of small celestial objects.<sup>3)</sup>

The estimated diameter of an asteroid is related to its reflectivity (quantified through its albedo,  $\alpha$ ) and brightness in the sky (quantified as the absolute magnitude,  $H$ ) through the following equation:

$$D = \frac{1329}{\sqrt{\alpha}} 10^{-0.2H} \quad (1)$$

Measuring the reflectivity, or albedo, of an asteroid generally requires an in-depth composition analysis best performed in-situ. As such, the size of an asteroid is most commonly estimated by its absolute magnitude alone,

with albedo approximated to be between 0.05 and 0.25 with an average of 0.1. Figure 1 below shows the approximate size range of detectable asteroids with absolute magnitudes between 20 and 25 (the lower limit of detection for most current ground-based telescopes).

The number of telescopes that can detect dim objects decreases with increasing magnitude, implying that there are very few telescopes currently able to detect objects with magnitudes above 21 – 22. This is why the catalogue of asteroids larger than 140 m has remained so limited.

The limited observability of these small asteroids leads to additional problems – namely, large orbit uncertainties following ground-based observation. With the detectability of dim objects improving with proximity to Earth, smaller objects are generally only observable within narrow encounter windows – typically less than a

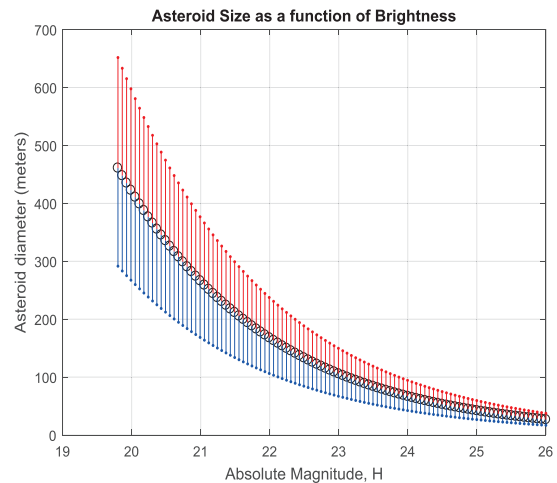


Figure 1: Approximate asteroid size as determined from absolute magnitude,  $H$ . Here, asteroid albedo is estimated to lie between 0.05 and 0.25.

few days. Orbit determination is improved by observing an appreciable section of an orbit period. With NEO asteroids' heliocentric periods often in the range of one to three years, a few days' worth of observations leads to observing less than 1% of an asteroid's orbit. While a given asteroid's position can be well determined with such a limited observation arc, the resultant orbit energy and velocity cannot.

Large initial orbit velocity uncertainties lead to poor position predictions in the future. This can be seen by propagating two states with an initially small difference in velocity. From the equation for orbit energy,

$$\varepsilon = \frac{v^2}{2} - \frac{GM}{r} \quad (2)$$

and taking the derivative of energy with respect to orbit velocity, one can see that orbit energy uncertainty is not only related to initial velocity uncertainty but also the orbit velocity at the time the uncertainty is found.

$$\Delta\varepsilon = v\Delta v \quad (3)$$

In other words, an orbit velocity uncertainty applied at periapsis will result in a larger position uncertainty compared to the same orbit uncertainty propagated from apoapsis. Figure 2 below shows an example of this difference. For this case, a heliocentric orbit with a 3.2-year orbit period was used. This orbit had an aphelion orbit velocity of about 10 km/s and a perihelion velocity of about 40 km/s. Figure 2 shows the resultant position uncertainty after one orbit with an uncertainty of only 10 cm/s applied at both orbit apses.

While this orbit is somewhat representative of the

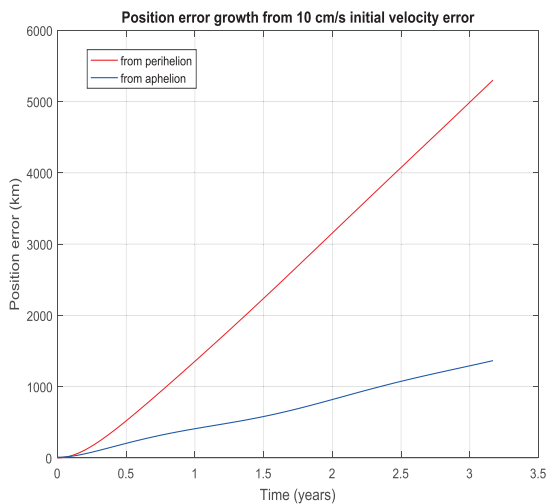


Figure 2: Position uncertainty growth from initial velocity uncertainty of 10 cm/s

family of PHAs currently catalogued, the achievable velocity uncertainty is highly dependent on the number of observations, the observation geometry, and a bevy of other factors. As such, typical velocity uncertainties can range widely from 5 to 10 cm/s up to 50 cm/s, resulting in position error growths anywhere between 500 km to 65,000 kilometers per year.

## 2.2. Risk Assessment Metrics

The risk posed to the Earth by a near-Earth asteroid (NEA) is often difficult to quantify. While simulations of the damage caused by asteroids of various sizes and composition are possible using atmospheric density models and complex fluid dynamics software, assessing

the likelihood of a particular impact requires direct observation of that asteroid along its orbit. Complicating this problem is that the ability to detect asteroids that may cause regional-level devastation is near the current limits of telescopic detection. As such, many PHAs have limited observations – leading to large orbit uncertainties. Propagating these uncertainties, say to a potential Earth impact, only causes the position uncertainty to grow, as was shown in the previous section. Hence, when the uncertainty contour is used to calculate the probability of collision ( $P_c$ ), the  $P_c$  value often comes back insignificantly small because the Earth’s volume subsumes so little of the uncertainty contour. Figure 3 shows the predicted position of the asteroid Apophis propagated from shortly after its discovery to the first possible Earth impact in 2029.

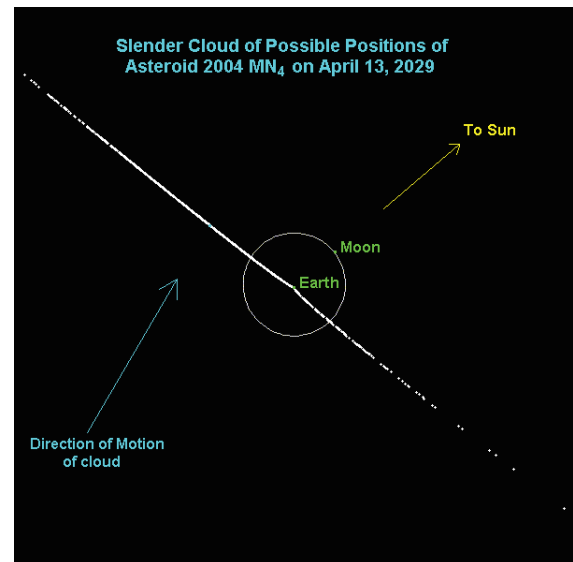


Figure 3: Image from NASA JPL Near Earth Object Program ([neo.jpl.nasa.gov/news/news146.html](http://neo.jpl.nasa.gov/news/news146.html))

This initial risk assessment of Apophis yielded a calculated  $P_c$  of only 0.33%.<sup>4)</sup> Such a small value could cause hesitancy if action were necessary. While it was later determined that Apophis posed no threat to Earth (it will still pass closer to Earth than many communication satellites), this may not be the case for future discoveries. One proposed improved metric for assessing risk was proposed via the use of the Mahalanobis distance.<sup>5)</sup> This calculation returns the number of standard deviations a point is from the center of a distribution. One benefit of this metric over  $P_c$  is the exclusion of a phenomenon referred to as “ $P_c$  roll-off.” This phenomenon is caused as the covariance matrix – the measure of the orbit uncertainty – collapses as a result of additional orbit

measurements. As such, the local probability density temporarily rises in the vicinity of the Earth, causing the  $P_c$  value to increase. In the Apophis case, additional measurements caused the covariance matrix to collapse close to the Earth, and the  $P_c$  rose to 2.7%.<sup>4)</sup> Eventually, additional observations caused the covariance to collapse beyond the surface of the Earth, and the  $P_c$  dropped to effectively zero. Conversely, an initial Mahalanobis distance calculation returns a  $\sigma$ -contour which would trend monotonically with subsequent measurements. Following the Apophis example, the initial risk assessment would have likely yielded  $1\sigma \leq D_{MH} \leq 2\sigma$ . This can be interpreted as having between a 1 in 3 and 1 in 22 chance of an impact. Subsequent measurements would have collapsed the covariance matrix, hence returning something like  $2\sigma \leq D_{MH} \leq 3\sigma$ , or between 1 in 22 and 1 in 370 chance of impact. Compare this to the increase of  $P_c$  from 0.33% to 2.7% using the same measurements.

### 3. Motivation and Approach

#### 3.1. Propagating through Gravity Gradients

It was found in Ref. 5) that propagating the covariance matrix through an Earth encounter period using only the state transition matrix caused the matrix to “teeter” or torque as it passed the Earth. As such, the leading and trailing edges of the matrix were stretched out and pivoted toward the Earth, causing the uncertainty distribution to shift its principal axes in the heliocentric frame from predominantly along-track prior to the encounter to predominantly cross-track afterward. The magnitude of the reorientation was dependent on two main factors: 1) how close the nominal trajectory passed by the Earth, and 2) how large the uncertainty distribution was prior to entering the Earth’s SOI.<sup>5)</sup>

#### 3.2. Miss Distances and Uncertainty Distributions

The reorientation of the covariance as it passed the Earth motivated analysis to relate the reorientation to Earth’s gravitational field. This analysis aimed to compare the largest eigenvalue of the analytical covariance matrix just prior to entering the Earth’s gravitational SOI to the asteroid’s minimum nominal miss distance with the Earth. The largest eigenvalue was used because this represents the largest spatial dimension of the uncertainty distribution. The minimum nominal miss distance was used as it implicitly relates to the largest gravitational magnitude that the distribution would encounter throughout its trajectory. The ratio of the eigenvalue and the minimum miss distance was in turn called the characteristic scale ratio, or  $R_{sc}$ .

To assess how well the uncertainty distribution remained Gaussian in Cartesian space, a Monte Carlo sampling of the covariance was compared to the analytical covariance propagated using a state transition matrix. Seven hundred and fifty samples were taken prior to the distribution entering the Earth’s SOI, when the leading sample was approximately 1.5 million km from the Earth. As both distributions were propagated across the Earth encounter, the percentage of samples that remained within each analytic  $\sigma$ -contour was determined via a  $D_{MH}$  calculation of each sample. This percentage was then compared against the expected percentages of a standard Gaussian distribution, shown below in Table 1.

Table 1: Expected proportion contained within various standard deviations of a Gaussian distribution

| $\sigma$ -contour           | Percentage contained |
|-----------------------------|----------------------|
| <b>1<math>\sigma</math></b> | 68.2689492%          |
| <b>2<math>\sigma</math></b> | 95.4499736%          |
| <b>3<math>\sigma</math></b> | 99.7300204%          |
| <b>4<math>\sigma</math></b> | 99.993666%           |
| <b>5<math>\sigma</math></b> | 99.9999426697%       |
| <b>6<math>\sigma</math></b> | 99.999998027%        |
| <b>7<math>\sigma</math></b> | 99.999999997440%     |

A covariance quality factor ( $C_{QF}$ ) was defined as the fraction of points that remained in the correct  $\sigma$ -contour. The  $C_{QF}$  was then used to assess how Gaussian a given sample set remained for a particular characteristic scale ratio. In this way, provided a particular  $R_{sc}$ , it was possible to determine which  $\sigma$ -contour was valid for a  $D_{MH}$  calculation to assess an asteroid’s impact risk.

### 4. Results and Conclusion

#### 4.1. Setup and Assumptions

For this analysis, the hypothetical impact scenario created for the 2015 Planetary Defense Conference was used.<sup>6)</sup> This scenario closely emulated the Chelyabinsk meteor trajectory and provided observation-based covariance information about the asteroid’s trajectory. From the scenario, the largest initial position and velocity eigenvalues were about 100 km and 7 cm/s, respectively.

To generate a data set for this analysis, two parameters needed to be varied: the amount of state uncertainty at the Earth encounter and the miss distance at TCA. First, to vary the scale of the uncertainty, the initial covariance was applied to the nominal trajectory at different times along its path. By applying the covariance along the asteroid’s trajectory as it came closer to Earth, the uncertainty had less time to grow. Hence, the scale of the covariance could be adjusted simply by adjusting

how long it was propagated. Second, to tailor the minimum nominal miss distance at TCA, small impulsive velocity perturbations were applied to the asteroid's orbit at the time the initial covariance was applied. By adjusting the magnitude of these velocity perturbations, it was possible to affect different miss distances. Generally, the greater the applied perturbation, the greater the nominal miss distance. By repeating this process at a number of different times along the asteroid's trajectory, it was possible to accumulate a representative set of characteristic scale ratios.

## 4.2. Results

Figure 4 below shows the  $7\sigma$  agreement between the Gaussian covariance matrix and the Monte Carlo samples for a subset of the cases examined. As previously mentioned, the characteristic ratio is the uncertainty scale divided by the minimum miss distance. Hence,  $R_{sc} = 10$  corresponds to a covariance matrix that is  $10\times$  larger than the minimum achieved miss distance over the encounter.

An initial assessment of Figure 4 shows that for  $R_{sc} \leq 104$ , the distributions appear to “rebound” to a

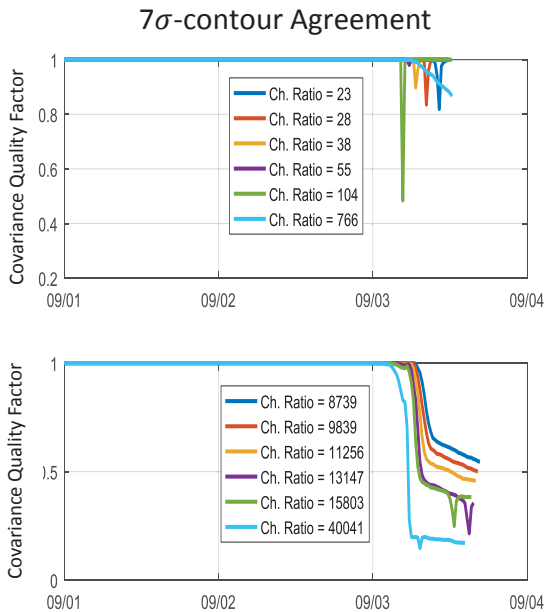


Figure 4: Covariance quality factor and characteristic scale ratio for different encounter trajectories

$7\sigma$  Gaussian agreement shortly after the encounter. Separately, for cases where  $R_{sc} \geq 766$ , the uncertainty distribution appears to continue to deteriorate from a Gaussian distribution following the encounter. This deterioration would thus imply that there exists values of  $R_{sc}$  between 104 and 766 where the uncertainty distribution no longer rebounds following the encounter.

Additionally, this figure suggests that for  $R_{sc} \leq 55$ , the  $7\sigma$  agreement remains above 80% with characteristic ratios around 55 showing a nearly 98% agreement with the Gaussian distribution.

Figure 5 below examines the minimum achieved covariance quality factor against the characteristic ratio. This comparison shows what appears to be an optimal characteristic ratio (better than 98% agreement) between values of 55 and 150.

These results are somewhat surprising as the expected relation was that the quality factor would monotonically improve with decreasing characteristic ratio. As such, it is possible that these results are a

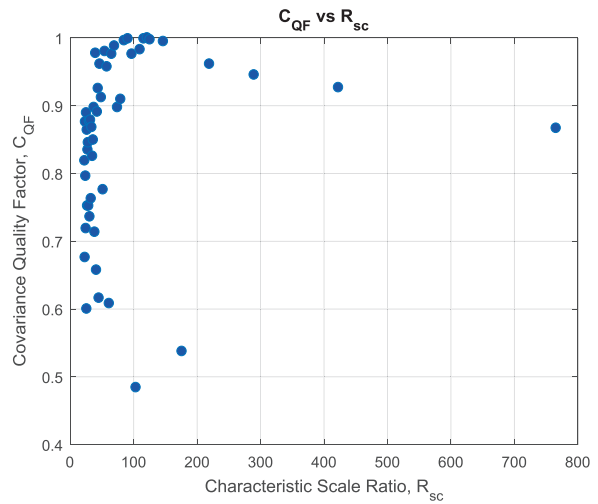


Figure 5: Covariance Quality Factor as a function of the Characteristic Scale Ratio

consequence of the limited samples examined thus far in the study. Specifically, the Earth encounter scenarios include a limited number of conjunction geometries where the relative orientation of the covariance is somewhat fixed based on the Earth's and asteroid's orbit alignment, despite earlier minor perturbations in the asteroid's trajectory. Extending the scenarios to include additional Earth-asteroid conjunction cases should improve these results. These results may also be a characteristic of the step-size granularity used for propagating the asteroid through the Earth encounter period. Smaller step-sizes may reveal much less peaked minima than are seen in these results. Repeated examinations for the  $6\sigma$ -,  $5\sigma$ -, and  $4\sigma$ -contours can be seen below in Figures 6, 7, and 8, respectively.

### 6 $\sigma$ -contour Agreement

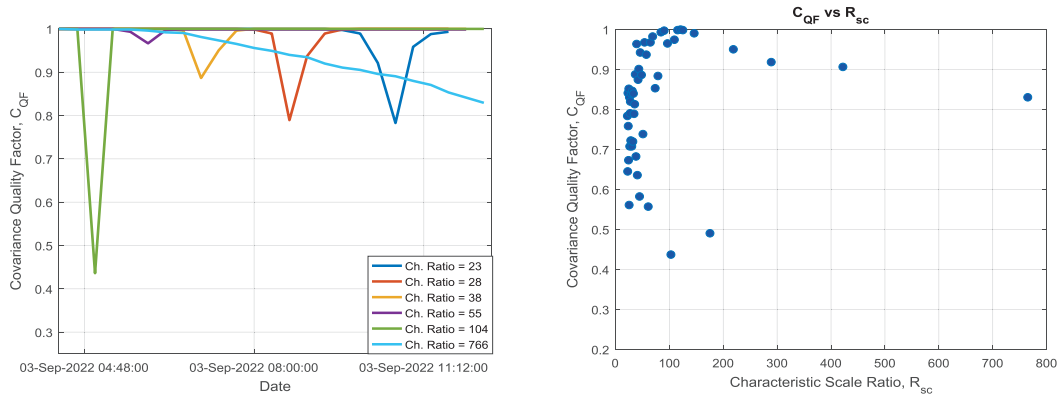


Figure 6: Covariance quality factor trending with time across Earth TCA (left) and minimum quality factor as a function of characteristic ratio (right)

### 5 $\sigma$ -contour Agreement

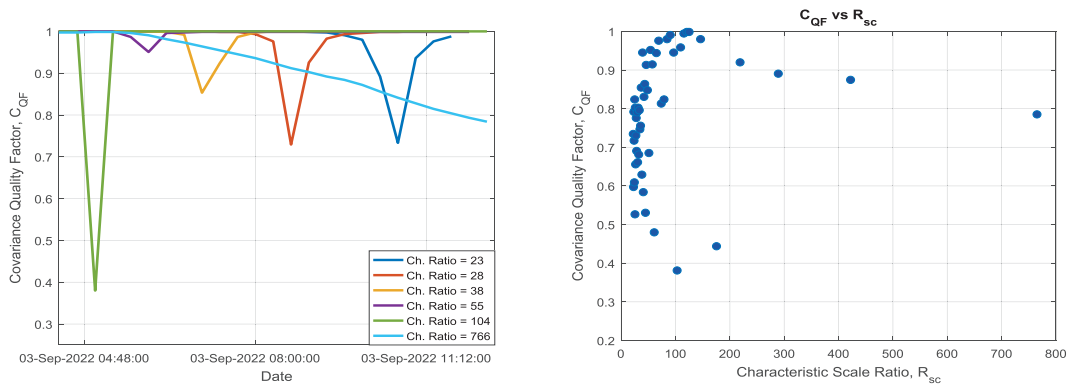


Figure 7: Covariance quality factor trending with time across Earth TCA (left) and minimum quality factor as a function of characteristic ratio (right)

### 4 $\sigma$ -contour Agreement

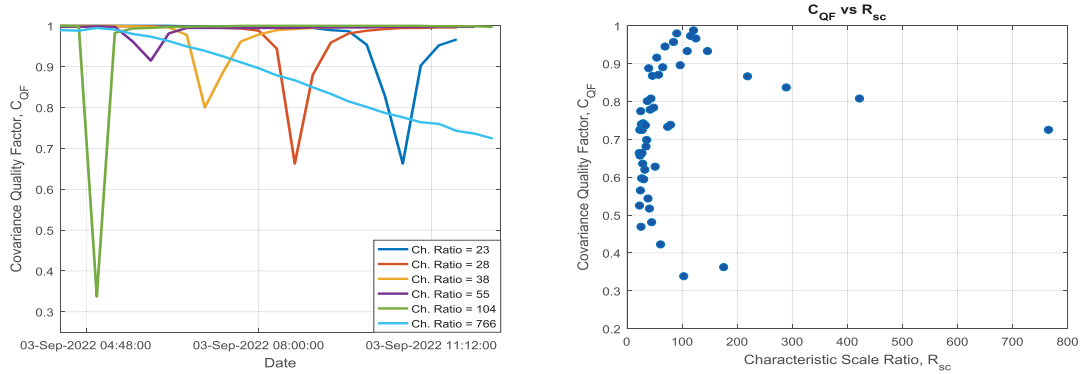


Figure 8: Covariance quality factor trending with time across Earth TCA (left) and minimum quality factor as a function of characteristic ratio (right)

As expected, these figures show that the quality degrades with decreasing  $\sigma$ -contours, implying that the distribution becomes less Gaussian closer to the nominal value. This result advocates a lower limit of around  $5\sigma$  when using a Mahalanobis metric for quantifying the impact risk of an asteroid, based on at least a 95% agreement with the Gaussian distribution.

## 5. Conclusions and Future Work

Preliminary results from this analysis suggest that  $D_{MH}$  calculations are a well suited risk metric for cases where  $R_{sc} \leq 150$ . However, this analysis also suggests that  $D_{MH}$  values below  $5\sigma$  are poorly representative of a Gaussian distribution. This can be seen qualitatively in Figures 9 and 10 below. In both figures, the top plot shows the 1-dimensional distance distribution between the Monte Carlo samples and Earth; the bottom plot shows the Monte Carlo samples of the covariance in the heliocentric, Cartesian frame. For a 3-dimensional, spatial Gaussian distribution, the corresponding distance distribution is also Gaussian for cases where the mean is much greater than the standard deviation ( $\mu \gg \sigma$ ). Hence, the top plot is very informative for how Gaussian the distribution remains after encountering the Earth. Both figures show the distributions a little more than two

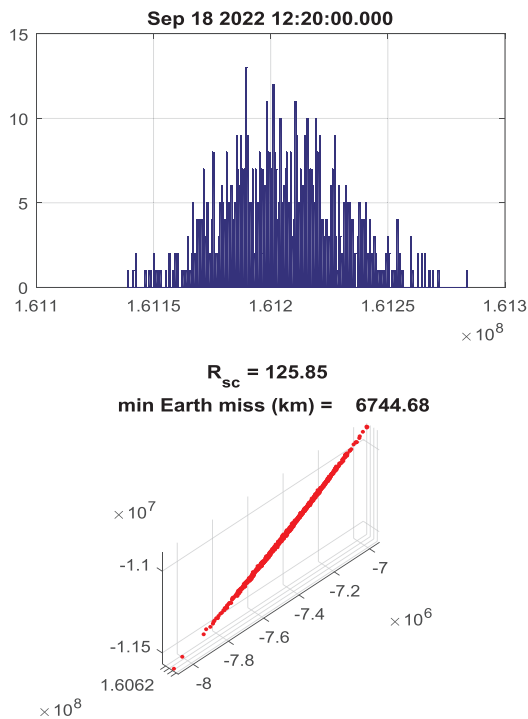


Figure 9: Distance distribution (top) and 3-dimensional position uncertainty (bottom)

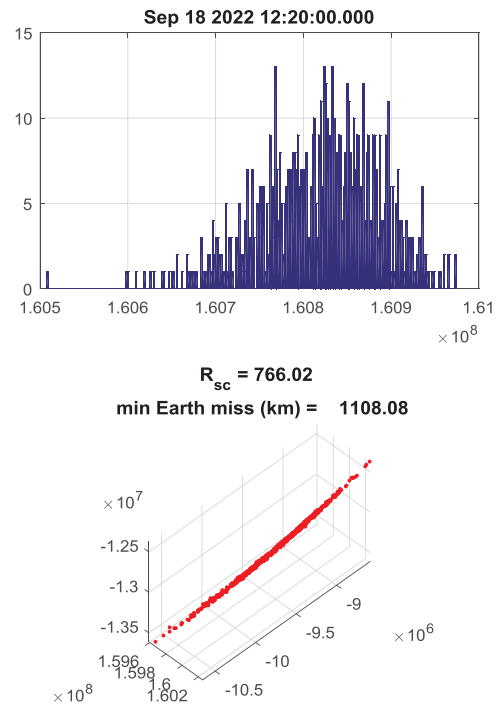


Figure 10: Distance distribution (top) and 3-dimensional position uncertainty (bottom)

weeks after encountering Earth, and an obvious tail can be seen in the histogram in Figure 10 – implying a poor Gaussian approximation for smaller  $\sigma$ -contours. For such cases where the uncertainty distribution does not remain Gaussian, a metric like  $P_c$  would still likely be necessary.

Future work is still needed to address the peaked minima shown in Figures 4, 6, 7, and 8. As stated previously, the sharp peaks are likely due to the step-size granularity during the Earth encounter period. Repeating the propagations with smaller step-sizes should rectify this issue. Additional asteroid trajectories will also need to be examined for this work to be complete. These trajectories will need to include a variety of relative velocity angles to capture different covariance orientations as the uncertainty distribution crosses through the Earth's gravitational field.

## References

- 1) Akella, M. and Alfriend, K.: *Probability of Collision Between Space Objects*, Journal of Guidance, Control, and Dynamics, Vol. 23, No. 5, September-October 2000
- 2) Mahalanobis, P. C.: *On the generalized distance in statistics*, Proceedings of the National Institute of Sciences of India, Vol. 2, No. 1, pp. 49-55, 1936

- 3) US National Science and Technology Council: *National Near-Earth Object Preparedness Strategy*, December 2016
- 4) Giorgini, J. D., et al: *Predicting the Earth encounters of (99942) Apophis*, [neo.jpl.nasa.gov/apophis/Apophis\\_PUBLISHED\\_PAPER.pdf](http://neo.jpl.nasa.gov/apophis/Apophis_PUBLISHED_PAPER.pdf), October 2008
- 5) Mattern, D.: *Deflection of an Earth-bound Asteroid using a Gravity-assisted Kinetic Impactor*, 2016 Astrodynamics Specialist Conference, September 2016
- 6) National Aeronautics and Space Administration Near Earth Object Program: *The 2015 PDC Hypothetical Asteroid Impact Scenario*, April 2015